DFT Studies of NH_3 Adsorption on Graphene-Supported Ni_xM_y (M=Pt and Rh; x=2–6; y=0–4)

Alfani Yusuf[1, 2], Adhitya Gandaryus Saputro [3], and Muhammad Haris Mahyudin[3,*]

[1]Master Program of Engineering Physics, Faculty of Industrial Technology, Institut Teknologi Bandung, Jl. Ganesha 10, Bandung, 40132, Indonesia.
[2]PLN Nusantara Power UMRO, Jl. Pluit Karang Ayu Barat No 1, 14450 Jakarta, Indonesia.
[3]Quantum and Nano Technology Research Group, Faculty of Industrial Technology, Institut Teknologi Bandung, 40132 Bandung, Indonesia.

*Email: mahyuddin133@itb.ac.id

Abstract. This study investigates the adsorption of ammonia (NH_3) on bimetallic Ni_xM_y-G (M = Pt, Rh; x = 2-6, y = 0-4) clusters supported on graphene using Density Functional Theory (DFT) calculations. The primary goal is to understand the structural stability and adsorption characteristics of these bimetallic clusters as potential catalysts for NH_3 decomposition, which plays a crucial role in hydrogen production. The results show that the substitution of nickel (Ni) atoms with platinum (Pt) or rhodium (Rh) improves the structural stability of the catalyst clusters, with Rh-based clusters showing greater stability than Pt-based ones. Furthermore, NH_3 adsorption tends to occur predominantly on Pt atoms in the Ni_xPt_y clusters and on Ni atoms in the Ni_xRh_y clusters. The strongest adsorption is observed in Ni_4Pt_2-G, indicating its high potential as a catalyst. Overall, the incorporation of Pt and Rh into Ni clusters enhances both stability and adsorption properties, positioning these bimetallic systems as promising candidates for further exploration in catalytic ammonia decomposition.

Keywords: *Density Functional Theory; Ammonia Adsorption; Nickel Cluster*

1 Introduction

Hydrogen has emerged as one of the promising candidates for CO_2 emission-free energy, offering potential as a replacement for fossil fuels [1]. The use of hydrogen is extensive, not only as a fuel for vehicles but also as a substitute for fossil fuels in various industries such as metal processing and petrochemicals. However, hydrogen still faces challenges in distribution and storage. To utilize hydrogen in the form of liquid hydrogen, an extremely low temperature of -252.76 °C at 1 atm is required, which demands a significant amount of energy.

Ammonia (NH_3) is currently one of the most promising candidates for hydrogen utilization. Ammonia can carry 18% wt of hydrogen, which is the highest among hydrogen carriers, and can be liquefied under milder conditions (-33.34°C at 1

Received _____, Revised _____, Accepted for publication _____

atm, or 20°C at 8.6 atm) [2]. The cost of utilizing ammonia is cheaper than using liquid hydrogen if ammonia is used directly in the final product. However, if the end-use product is hydrogen, costs increase by 26.5% due to the decomposition process, which requires high temperatures (400-700°C at 1 atm) [3].

Several transition metals have been tested for their performance as catalysts in the ammonia decomposition process, including Ru, Ir, Rh, Pt, Pd, Ni, Co, and Fe [4–9]. Among these, Ru has been identified as the most active catalyst. Mainly, ruthenium supported on carbon nanotubes (CNT) has been found to be the most active catalyst due to its high conductivity. Additionally, the rate of NH_3 decomposition highly depends on the size and shape of Ru nanoparticles [10]. However, ruthenium is a precious metal and is therefore very expensive. For practical applications, the amount of Ru in the catalyst must be reduced, or Ru must be replaced with a more affordable metal.

Among non-precious metals, Ni has gained attention due to its better activity compared to other non-precious metals such as Fe and Co [9]. A first-principles study conducted by Wei Guo et al. investigated bimetallic catalysts made of Ni nanoparticles on a Pt surface for ammonia decomposition [11]. The study found that Ni terrace sites facilitate N–H bond cleavage, while Ni edge sites support the association of atomic nitrogen into nitrogen molecules (N_2). At Ni percentages below 50%, the Ni-Pt bimetallic catalyst remained effective due to active surface sites. At Ni levels close to 50%, there is an optimal balance between terrace sites (for N-H dissociation) and edge sites (for N-N association), resulting in the highest turnover frequency (TOF). If the Ni percentage is too high or too low, catalyst efficiency decreases due to the reduced dominance of one of the active sites.

Meng Miao et al., using density functional theory (DFT) calculations, compared the energy barriers for ammonia decomposition on Ni_6 and Ni_6-G clusters [12]. The study showed a decrease in the activation energy for N recombination into N_2 (the rate-determining step, RDS) from 2.25 eV on Ni_6 to 1.47 eV on Ni_6-G. Additionally, Meng Miao et al. conducted a theoretical study on other ammonia decomposition catalysts using Fe-based bimetallic alloys with the addition of Mo, Ni, and Pt supported by graphene [7]. The study found that these Fe-M bimetallic alloys could enhance adsorption and catalytic activity compared to Fe-based catalysts alone. The adsorption energy of NH_3 decreased from -1.00 eV for Fe alone to -1.09 eV for Fe_5Pt, Fe_5Mo, and -1.03 eV for Fe_5Ni. This reduction in adsorption energy accelerates the TOF. The energy barrier for N+N recombination, which is the RDS, was also reduced by these alloys: from 2.86 eV for Fe to 2.57 eV for Fe-Mo, 2.28 eV for Fe-Ni, and 1.75 eV for Fe-Pt.

In this study, we combined DFT calculations and microkinetic simulation to investigate the structure and stability of bimetallic Ni_xM_y clusters supported on graphene (M=Pt and Rh; x=2–6, y=0–4) to understand ammonia adsorption, which is a crucial initial step in ammonia decomposition into hydrogen and nitrogen.

2 Methodology

A Ni_6 atomic cluster placed on a graphene supercell with dimensions of a = 14.757 Å, b = 12.78 Å, and a vacuum space of 15 Å above the graphene surface was utilized for calculations. The Ni_6 cluster structure adequately accommodates all steps in the decomposition process of ammonia into nitrogen and hydrogen. Variation of bimetallic Ni_xM_y clusters were formed by substituting Ni atoms with Pt and Rh atoms, resulting in Ni_5Pt, Ni_4Pt_2, Ni_3Pt_3, Ni_2Pt_4, Ni_5Rh, Ni_4Rh_2, Ni_3Rh_3, and Ni_2Rh_4, all supported on graphene. One ammonia molecule was placed on the optimized Ni_xM_y-G catalysts to identify the most stable ammonia adsorption site.

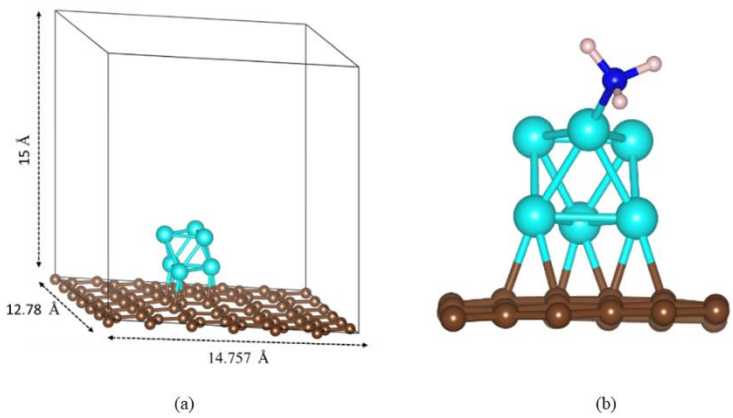

Figure 1 (a) Structure Ni_6-G (b) NH_3 adsorp on Ni_6-G

Spin-polarized calculations using the Kohn–Sham formulation [13, 14] as implemented in Vienna Ab-initio Simulation Package (VASP) version 5.4.4 [15, 16] was used for all calculations. The Projector Augmented Wave (PAW) method described the interaction between the core and electrons [17, 18]. Electron exchange correlation was treated with the Perdew-Burke-Ernzerhof (PBE) function based on the generalized gradient approximation (GGA) [19]. A plane-wave basis set with a cut-off energy of 500 eV, with a total energy convergence set at 1×10^{-5} eV for electronic iterations and force convergence for each ionic iteration was set below 0.03 eV $Å^{-1}$. The Brillouin zone was sampled using a

Monkhorst-Pack 3×3×1 k-point mesh [20]. The zero-damping D3 method of Grimme was applied to account for dispersion corrections [21]. Geometry optimization was performed using the conjugate gradient method. Calculations were considered converged when the maximum force on the unconstrained atoms was below 0.03 eV/Å. Atomic charges and spin densities were computed using the Bader charge analysis algorithm, and the optimized structures were visualized using VESTA [22].

The binding energy (E_b) of Ni_xM_y on graphene sheet was calculated using equation 1 [23].

$$E_b = E_{NixMy-G} - \left(E_{NixMy} + E_{graphene}\right) \quad (1)$$

where, $E_{NixMy@grafena}$, E_{NixMy}, $E_{(graphene)}$ are the total energies of Ni_xM_y cluster on graphene sheet, the cluster; the graphene sheet, respectively. The NH_3 adsorption energy (E_{ads}) was calculated using equation 2 [23].

$$E_{ads} = E_{system} - \left(E_{NixMy-G} + E_{NH3}\right) \quad (2)$$

where E_{system} and E_{NH3} are the total energies of NH_3 adsorbed on the system and an isolated NH_3 molecule, respectively.

3 Result and discussion

3.1 Stability Structure Ni_xM_y-G

As shown in Figure 2, the Ni_6-G catalyst exhibited the highest energy. The substitution of Ni atoms with Pt and Rh reduced energy and increased structural stability in the catalyst cluster material. The energy reduction in the Ni_xRh_y-G structure was more significant than in the Ni_xPt_y-G structure. The calculated E_b showed the order of the binding strength of N_xM_y on graphene as Ni_3Rh_3-G > Ni_3Pt_3-G > Ni_4Rh_2-G > Ni_4Pt_2-G > Ni_2Rh_4-G > Ni_2Pt_4-G > Ni_5Rh-G > Ni_5Pt-G > Ni_6-G, suggesting that substitution of Pt or Rh on Ni_6 cluster increases the stability binding clusters catalyst on graphene.

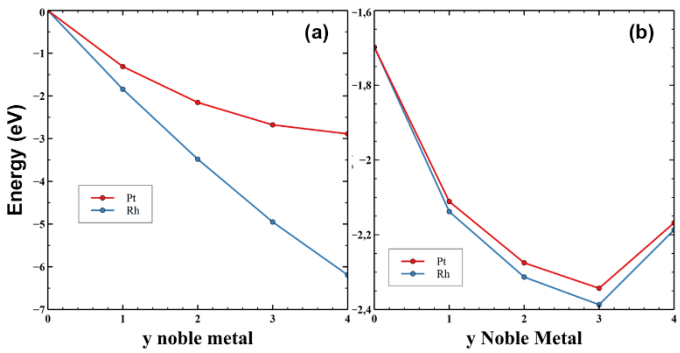

Figure 2 (a) Relative Energy of the Ni_xM_y-G catalyst compared to Ni_6-G (b) Binding Energy of Ni_xM_y-G.

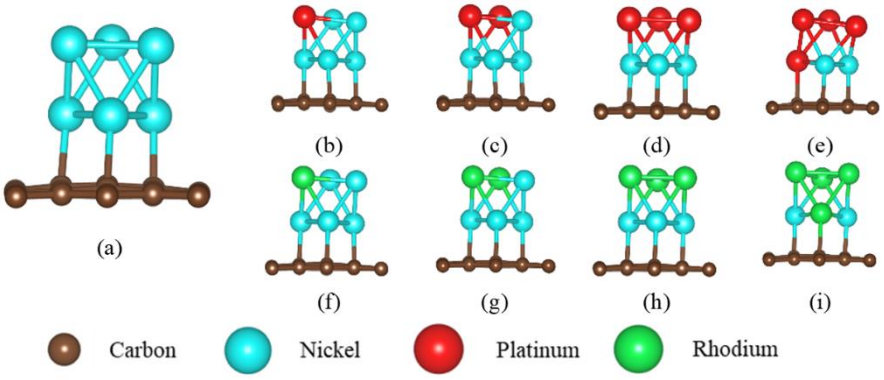

Figure 3 Optimized geometries of (a) Ni_6-G, (b) Ni_5Pt-G, (c) Ni_4Pt_2-G, (d) Ni_3Pt_3-G, (e) Ni_2Pt_4-G, (f) Ni_5Rh-G, (g) Ni_4Rh_2-G, (h) Ni_3Rh_3-G, (i) Ni_2Rh_4-G

Table 1 Selected bond lengths for all studied catalysts.

Ni_xM_y-G	Bond Length (Å)					
	Ni-Ni	**Ni-Pt**	**Ni-Rh**	**Pt-Pt**	**Rh-Rh**	**Ni-C**
Ni_6	2.35	**	**	**	**	2.07
Ni_5Pt	2.41	2.46	**	**	**	2.06
Ni_4Pt_2	2.42	2.45	**	2.63	**	2.06
Ni_3Pt_3	2.42	2.47	**	2.64	**	2.07
Ni_2Pt_4	2.45	2.50	**	2.63	**	2.08
Ni_5Rh	2.40	**	2.40	**	**	2.07
Ni_4Rh_2	2.40	**	2.430	**	2.46	2.09
Ni_3Rh_3	2.42	**	2.435	**	2.46	2.11
Ni_2Rh_4	2.54	**	2.453	**	2.46	2.12

The optimized geometries of all studied catalysts are presented in Figure 3. There is a noticeable change in bond lengths between atoms. In the Ni_6 structure, the bond length between Ni atoms is 2.35 Å, and the bond length between Ni atoms and carbon atoms in graphene is 2.07 Å. Substituting Ni atoms with Pt atoms increases the Ni-Ni bond length to 2.41 and 2.45 Å in Ni_5Pt-G Ni_2Pt_4-G, respectively. Similarly, the Ni-Pt bond length also tends to increase as more Ni atoms are replaced by Pt, from 2.46 Å in Ni_5Pt-G to 2.50 Å in Ni_2Pt_4-G. The Pt-Pt bond has the most significant bond length of 2.35 Å, and there is no significant change with the increased Pt content in the catalyst material structure. This increase in bond lengths between atoms causes the Ni_6 cluster size to expand as Pt substitutes more Ni atoms. In the Ni_xRh_y-G structure, the Ni-Ni bond length

increases, as do the Ni-Rh and Rh-Rh bond lengths, which are longer than the Ni-Ni bonds in Ni_6-G. This makes the Ni_xRh_y-G cluster more prominent than the Ni_6 cluster structure.

3.2 NH_3 Adsorption on N_xM_y-G

Figure 4 shows the most energetically favorable adsorption site for ammonia on the Ni_xM_y-G catalysts. On the Ni_xPt_y-G, the adsorption energy tends to be more negative as the number of Pt atoms increases, indicating stronger NH_3 adsorption on the catalyst. An exception is observed in Ni_5Pt-G, where the adsorption energy is only -1.32 eV, which is higher than Ni_6-G (-1.43 eV). Ammonia adsorption generally occurs on Pt atoms, except for Ni_5Pt-G, where adsorption is more favorable on Ni atoms.

In contrast, for Ni_xRh_y-G catalysts, NH_3 adsorption tends to occur on Ni atoms rather than Rh, except in Ni_2Rh_4-G, where adsorption occurs on Rh atoms. All NH_3 adsorption energies on Ni_xRh_y-G are greater than those on Ni_6-G. The order of NH_3 adsorption strength from strongest to weakest is as follows: Ni_4Pt_2-G > Ni_3Pt_3-G > Ni_4Pt_2-G > Ni_2Rh_4-G > Ni_6-G > Ni_5Pt-G > Ni_5Rh-G > Ni_2Rh_4-G.

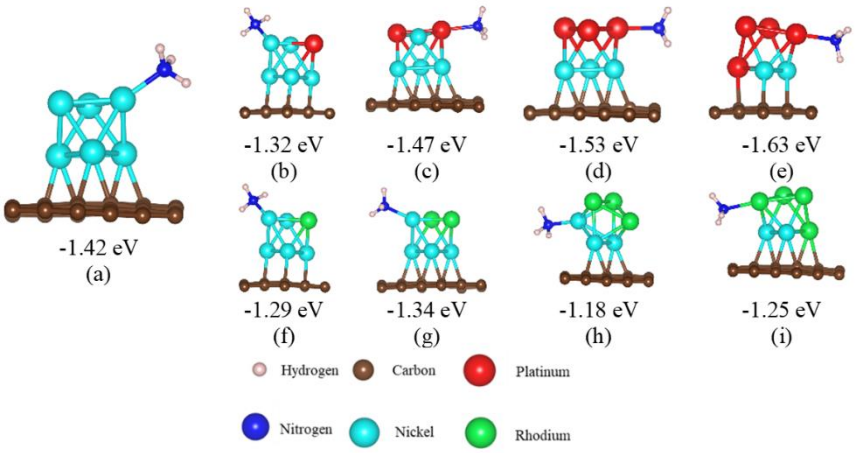

Figure 4 Calculated NH_3 adsorption energies and sites on (a) Ni_6-G, (b) Ni_5Pt-G, (c) Ni_4Pt_2-G, (d) Ni_3Pt_3-G, (e) Ni_2Pt_4-G, (f) Ni_5Rh-G, (g) Ni_4Rh_2-G, (h) Ni_3Rh_3-G, and (i) Ni_2Rh_4-G.

3.3 PDOS Analysis

Having understood that ammonia tends to adsorb more on platinum, followed by nickel, and then rhodium, we show in Figure 5 PDOS analysis of NH_3 adsorption

on Ni_2Pt_4-G, Ni_6-G, Ni_3Rh_3-G (on Ni), and Ni_3Rh_3-G (on Rh) to obtain more insights into these intriguing results.

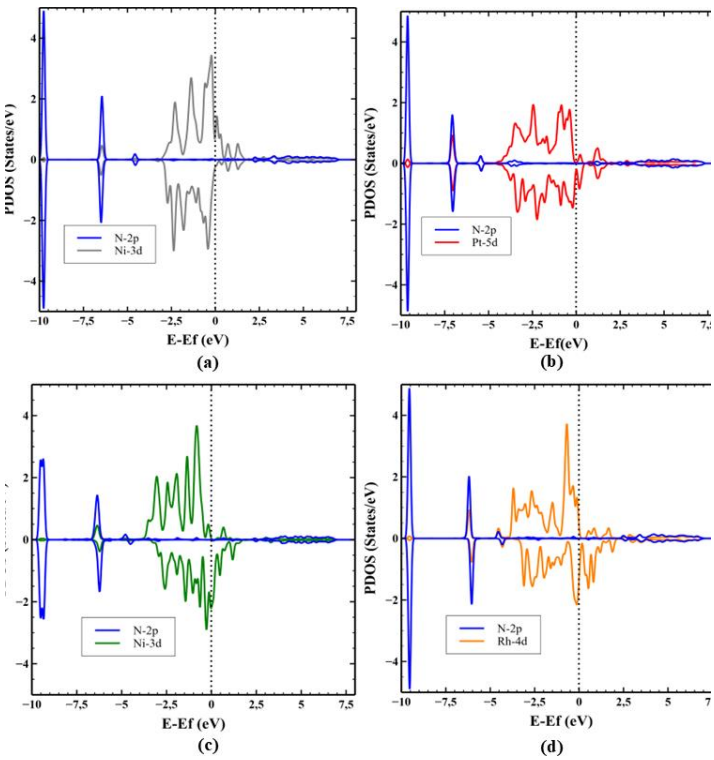

Figure 5 PDOS NH_3 adsorption on (a) Ni_6-G (b) Ni_2Pt_4-G (c) Ni_3Rh_3-G(on Ni) (d) Ni_3Rh_3-G(on Pt).

N-2p states in both systems show peaks at similar energies (about -7.5 eV), indicating similar adsorption energy of nitrogen on both surfaces. The Ni-3d states at Ni_6-G show a broad distribution near the Fermi level ($E-E_F = 0$), which suggests metallic character for the nickel. However, there is no significant overlap between the N-2p and Ni-3d states near the Fermi level, implying that the N atom may not be strongly hybridizing with the nickel orbitals at the Fermi level. In this case Ni_2Pt_4-G, the Pt-5d states show stronger contributions both below and above the Fermi level, with notable states near 0 eV. This suggests significant metallic character and possible hybridization with N-2p states, especially around the Fermi level. Compared to the Ni surface, there appears to be more overlap between the N-2p and Pt-5d states near the Fermi level, suggesting a potentially stronger interaction between ammonia and the Pt sites compared to Ni.

In Ni_3Rh_3-G, the Ni-3d states exhibit a wide distribution from -6 to 2.5 eV, with several significant peaks around the Fermi level. This broad range of Ni-3d states

indicates strong metallic character, and more importantly, the overlap between Ni-3d and N-2p states near the Fermi level suggests hybridization, meaning the ammonia molecule is interacting strongly with the nickel atoms at the surface. In Figure 5d, the Rh-4d states show a broad distribution, mainly concentrated from -6 to about 2 eV, but the significant Rh-4d states near the Fermi level are less prominent compared to the Ni-3d states in the Figure 5c. This lower density of Rh-4d states around the Fermi level suggests a weaker interaction between the Rh-4d and N-2p states.

4 Conclusion

NH_3 adsorption over Ni_xM_y-G (M= Pt, Rh; x=2-6, y= 0-4) was explored using DFT calculations. The substitution of Ni atoms with Pt or Rh atom in the Ni_xM_y clusters improved the structural stability of the catalyst, with Ni-Rh combinations showing more significant stability than Ni-Pt combinations. The NH_3 adsorption strength varied across different bimetallic clusters. NH_3 adsorbed more strongly on Pt atoms in Ni_xPt_y clusters, while in Ni_xRh_y clusters, adsorption tended to occur on Ni atoms. The highest adsorption energy was observed in Ni_4Pt_2-G, indicating that this structure had the strongest NH_3 interaction. The substitution of Ni with Pt or Rh increased the bond lengths of the clusters, which also influenced the NH_3 adsorption characteristics. In conclusion, the present study demonstrated that incorporating Pt and Rh into Ni-based bimetallic clusters significantly enhances both the stability and adsorption properties, with Pt-rich clusters offering the strongest adsorption for ammonia, making them promising candidates for further research in the catalytic decomposition of NH_3 to H_2.

5 References

[1] R. Lan, J. T. S. Irvine, and S. Tao., *Ammonia and related chemicals as potential indirect hydrogen storage materials*, International Jurnal of Hydrogen Energy, **37**(2), pp. 1482-1494, Jan. 2012, doi: 10.1016/j.ijhydene.2011.10.004.

[2] M. Aziz, T. Oda, and T. Kashiwagi., *Comparison of liquid hydrogen, methylcyclohexane and ammonia on energy efficiency and economy*, *Energy Procedia.*, pp. 4086-4092, 2019, doi: 0.1016/j.egypro.2019.01.827.

[3] Xuezhi Duan, Ji Jian, Qian Gang, Fan Chen, Zhu Yian, Xinggui Zhoua, De Chen, & Weikang Yuana, *Ammonia decomposition on Fe(1 1 0), Co(1 1 1) and Ni(1 1 1) surfaces: A density functional theory study*, Journal of Molecular Catalysis A: Chemical, **357**, pp. 81–86, May. 2012, doi: 10.1016/j.molcata.2012.01.023.

[4] D. A. Hansgen, D. G. Vlachos, and J. G. Chen, *Using first principles to predict bimetallic catalysts for the ammonia decomposition reaction*, Nature Chemistry, **2**(6), pp. 484–489, Jun. 2010, doi: 10.1038/nchem.626.

[5] J. Łuczak and M. Lieder, *Nickel-based catalysts for electrolytic decomposition of ammonia towards hydrogen production*, Advances in Colloid and Interface Science, **319**(102993), Sep. 2023, doi: 10.1016/j.cis.2023.102963.

[6] X. HAN, W. CHU, P. NI, S. LUO, and T. ZHANG, *Promoting effects of iridium on nickel based catalyst in ammonia decomposition*, Journal of Fuel Chemistry and Technology, **35**(6), pp. 691–695, Dec. 2007, doi: 10.1016/S1872-5813(08)60004-3.

[7] M. Miao, M. Sha, C. Cao, S. Lei, and Q. Meng, *Theoretical study on Fe-M (M = Mo, Ni, Pt) bimetallic catalysts to promote ammonia decomposition*, Chemical Physics Letters, **808**(140134), Dec. 2022, doi: 10.1016/j.cplett.2022.140134.

[8] H. Fang, Liu Dan, Luo Yu, Zhou Yanliang, Wang Xiuyun, Lin Bingyu, & Jiang Lilong, *Challenges and Opportunities of Ru-Based Catalysts toward the Synthesis and Utilization of Ammonia*, American Chemical Society, **12**(7), pp. 3938-3954, Apr. 2022, doi: 10.1021/acscatal.2c00090.

[9] Tianxu Su, Bin Guan, et al., *Review on Ru-Based and Ni-Based Catalysts for Ammonia Decomposition: Research Status, Reaction Mechanism, and Perspectives*, Energy and Fuels, **37**(12), pp. 8099-8127, Jun. 2023, doi: 10.1021/acs.energyfuels.3c00804.

[10] S. Zhou, S. Lin, and H. Guo, *First-Principles Insights into Ammonia Decomposition Catalyzed by Ru Clusters Anchored on Carbon Nanotubes: Size Dependence and Interfacial Effects*, Journal of Physical Chemistry C, **122(**16), pp. 9091–9100, Apr. 2018, doi: 10.1021/acs.jpcc.8b01965.

[11] W. Guo and D. G. Vlachos, *Patched bimetallic surfaces are active catalysts for ammonia decomposition*, Nature Communications, **6**(8619), Oct. 2015, doi: 10.1038/ncomms9619.

[12] M. Miao, X. Gong, S. Lei, L. Wang, M. Sha, and Q. Meng, *The graphene-supported non-noble metal catalysts activate ammonia decomposition: A DFT study*, Chemical Physics, **548**(111249), Aug. 2021, doi: 10.1016/j.chemphys.2021.111249.

[13] P. Hohenberg and W. Kohn, *Inhomogeneous Electron Gas*, Physical Review, **136(**3B), pp. B864–B871, Nov. 1964, doi: 10.1103/PhysRev.136.B864.

[14] W. Kohn and L. J. Sham, *Self-Consistent Equations Including Exchange and Correlation Effects*, Physical Review, **140 (**4A), pp. A1133–A1138, Nov. 1965, doi: 10.1103/PhysRev.140.A1133.

[15] G. Kresse and J. Furthmüller, *Efficiency of ab-initio total energy calculations for metals and semiconductors using a plane-wave basis set*,

Computational Materials Science, **6(**1), pp. 15–50, Jul. 1996, doi: 10.1016/0927-0256(96)00008-0.

[16] G. Kresse and J. Furthmüller, *Efficient iterative schemes for ab initio total-energy calculations using a plane-wave basis set*, Physical Review B, **54**(16), pp. 11169–11186, Oct. 1996, doi: 10.1103/PhysRevB.54.11169.

[17] P. E. Blöchl, *Projector augmented-wave method*, Physical Review B, **50(**24), pp. 17953–17979, Dec. 1994, doi: 10.1103/PhysRevB.50.17953.

[18] G. Kresse and D. Joubert, *From ultrasoft pseudopotentials to the projector augmented-wave method*, Physical Review B, **59**(3), pp. 1758–1775, Jan. 1999, doi: 10.1103/PhysRevB.59.1758.

[19] J. P. Perdew, K. Burke, and M. Ernzerhof, *Generalized Gradient Approximation Made Simple*, Physical Review Letters, **77**(18), pp. 3865–3868, Oct. 1996, doi: 10.1103/PhysRevLett.77.3865.

[20] H. J. Monkhorst and J. D. Pack, *Special points for Brillouin-zone integrations*, Physical Review B, **13(**12), pp. 5188–5192, Jun. 1976, doi: 10.1103/PhysRevB.13.5188.

[21] S. Grimme, *Semiempirical GGA-type density functional constructed with a long-range dispersion correction*, Journal of Computational Chemistry, **27**(15), pp. 1787–1799, Nov. 2006, doi: 10.1002/jcc.20495.

[22] K. Momma and F. Izumi, *VESTA 3 for three-dimensional visualization of crystal, volumetric and morphology data*, Journal of Applied Crystallography, **44**(6), pp. 1272–1276, Dec. 2011, doi: 10.1107/S0021889811038970.

[23] D. S. Sholl and J. A. Steckel, *Density functional theory: a practical introduction*. John Wiley & Sons, 2022.

Acknowledgement

This work was supported and funded by PT PLN Persero, PT PLN Nusantara Power, and the Directorate of Research and Development Universitas Indonesia (DRP UI) and the Directorate of Research and Community Service Institut Teknologi Bandung (DRPM ITB) under Hibah UI-ITB BiSA 2024 (grant no. 8331/IT1.B07.1/TA.00/2024).